NASA TECHNICAL NOTE

NASA TN D-6188

ROLE OF HYDROGEN IN HOT-SALT STRESS-CORROSION OF A TITANIUM ALLOY

by Hugh R. Gray

Lewis Research Center

Cleveland, Ohio 44135

NATIONAL AERONAUTICS AND SPACE ADMINISTRATION • WASHINGTON, D. C. • FEBRUARY 1971

1. Report No.	2. Government Accession No.	3. Recipient's Catalog No.
NASA TN D-6188		

4. Title and Subtitle

ROLE OF HYDROGEN IN HOT-SALT STRESS-CORROSION OF A TITANIUM ALLOY

5. Report Date: February 1971

6. Performing Organization Code:

7. Author(s)

Hugh R. Gray

8. Performing Organization Report No.: E-5960

9. Performing Organization Name and Address

Lewis Research Center
National Aeronautics and Space Administration
Cleveland, Ohio 44135

10. Work Unit No.: 129-03

11. Contract or Grant No.:

12. Sponsoring Agency Name and Address

National Aeronautics and Space Administration
Washington, D.C. 20546

13. Type of Report and Period Covered: Technical Note

14. Sponsoring Agency Code:

15. Supplementary Notes

16. Abstract

Corrosion-produced hydrogen was confirmed as the embrittling species during hot-salt stress-corrosion of titanium alloys. Local concentrations of hydrogen of several thousand ppm were measured on a microscopic scale. These local hydrogen contents were substantially greater than the average bulk values (100 ppm) measured in salt-corroded specimens. Concentrations of hydrogen similar to the measured local values were charged into as-received Ti-8Al-1Mo-1V alloy specimens. These charged specimens were brittle when tensile tested at 800° F (427° C), as were the hot-salt stress-corroded specimens.

17. Key Words (Suggested by Author(s))	18. Distribution Statement
Hydrogen embrittlement; Hot-salt stress-corrosion; Stress-corrosion; Titanium alloy; Mass spectrometer	Unclassified - unlimited

19. Security Classif. (of this report)	20. Security Classif. (of this page)	21. No. of Pages	22. Price*
Unclassified	Unclassified	28	$3.00

*For sale by the National Technical Information Service, Springfield, Virginia 22151

ROLE OF HYDROGEN IN HOT-SALT STRESS-CORROSION OF A TITANIUM ALLOY

by Hugh R. Gray

Lewis Research Center

SUMMARY

Previous research had confirmed that hydrogen is produced and absorbed by titanium alloys during a hot-salt stress-corrosion exposure. This hydrogen then embrittles the alloy specimens when they are mechanically tested at low strain rates near ambient temperature. The purpose of this investigation was to study the role of hydrogen in promoting embrittlement at elevated temperatures, where the process of hot-salt stress-corrosion occurs.

Salt-coated specimens of the Ti-8Al-1Mo-1V alloy were subjected to low-strain-rate tensile tests, creep exposure tests, and stress-rupture tests to demonstrate the effects of hot-salt stress-corrosion. Severe embrittlement and/or cracking was observed in all types of tests. Significant increases in hydrogen concentrations in stress-corroded specimens were measured by standard vacuum-fusion chemical techniques. Ion-probe mass-spectrometric techniques revealed that hydrogen was segregated near the fracture surface to extremely high concentrations (several thousand ppm). These high concentrations were duplicated by thermal hydrogenation of the as-received Ti-8Al-1Mo-1V alloy specimens. These were brittle when tensile tested at 800° F (427° C). Salt-coated specimens were also brittle when tested under identical tensile conditions.

INTRODUCTION

The phenomenon of hot-salt stress-corrosion of titanium alloys is of interest because of extensive use of titanium alloys in the compressors of jet turbine engines. Numerous laboratory investigations (ref. 1) have demonstrated that titanium alloys are susceptible to embrittlement and cracking at elevated temperatures while being stressed in the presence of halides. Similar conditions of stress, temperature, and salt-air environment can be experienced by compressor components of current engines (ref. 2).

Since advanced engine designs specify that titanium alloys operate at even higher stresses and temperatures, there is concern that hot-salt stress-corrosion might become the limiting factor in the use of titanium alloys. To date, there have not been any reported service failures that could conclusively be attributed to hot-salt stress-corrosion. However, neither the lack of service failures nor the mechanism of embrittlement encountered in laboratory tests has been completely rationalized.

One of the more preferred laboratory test techniques for determining susceptibility to hot-salt stress-corrosion involves subjecting salt-coated titanium alloy specimens to static loads. The test temperatures range from 500° to 900° F (260° to 480° C) and the test duration is generally 100 hours. The specimens are then examined for evidence of corrosion or cracking, and may be subjected to mechanical testing, such as bend or tensile testing, to determine residual ductility. The results are then interpreted on a stress-corrosion or no-stress-corrosion basis. Thus, the boundary line separating regions of cracking from no-cracking or embrittlement from nonembrittlement on a plot of exposure stress against exposure temperature has been termed the threshold curve for hot-salt stress-corrosion.

Several investigators (refs. 3 to 5) have suggested that hot-salt stress-corrosion of titanium alloys may be a result of hydrogen embrittlement. Corrosion reactions involving titanium, salt, oxygen, and moisture and resulting in the generation of hydrogen have been postulated (refs. 3, 6, and 7). Radioactive-tracer techniques have been used to demonstrate that corrosion-produced hydrogen concentrates in salt-corroded areas (refs. 3 and 8). Direct observation of hot-salt stress-corrosion by hot-stage metallography has revealed that cracks initiated abruptly after an incubation period (ref. 9). Additional evidence that suggests a hydrogen embrittlement mechanism is the demonstrated ability to retard cracking by applied anodic potentials (ref. 4).

This author has recently confirmed (ref. 10) that corrosion-produced hydrogen is responsible for the temperature and strain-rate sensitivity observed during postexposure tensile testing of the Ti-8Al-1Mo-1V alloy. Briefly, embrittlement was found to be most severe at low strain rates and at temperatures close to room temperature. Direct measurements were made that showed increased hydrogen concentrations in stress-corroded specimens. Removal of hydrogen from stress-corroded specimens by vacuum annealing resulted in full recovery of ductility. These results confirmed that hydrogen was generated and absorbed by the alloy during an 800° F (427° C) stress-corrosion exposure. Hydrogen was then responsible for the embrittlement observed during subsequent mechanical testing near room temperature.

However, as will be shown, the results of postexposure mechanical testing at room temperature are not the only manner in which stress-corrosion damage is revealed. In fact, titanium alloy specimens will crack and even rupture in a brittle manner at elevated temperatures, if the exposure stress levels are well above the embrittlement

threshold, and/or if the exposure time is extended beyond 100 hours. The specific mechanism by which hydrogen promotes cracking at elevated temperatures is not clear. It could even be postulated that since both titanium alloy solubility for hydrogen and the diffusion rate of hydrogen increase with increasing temperature, it is not likely that hydrogen could segregate to concentration levels that would promote cracking. The purpose of this investigation was to determine whether hydrogen could embrittle titanium alloys in the temperature range where hot-salt stress-corrosion is known to occur.

Salt-coated specimens of the Ti-8Al-1Mo-1V alloy were subjected to elevated-temperature tensile tests, creep exposure tests, and stress-rupture tests to establish the effects of hot-salt stress-corrosion. Evidence of embrittlement and/or cracking was sought in all types of tests. Standard vacuum-fusion chemical techniques were used to determine significant increases in hydrogen concentrations. Ion-probe mass-spectrometric techniques were used to determine if hydrogen were segregated near the fracture surface in extremely high concentrations. High surface concentrations of hydrogen were duplicated by thermal hydrogenation methods. These hydrogenated specimens were mechanically tested at elevated temperatures to determine if embrittlement had occurred.

MATERIAL, SPECIMENS, AND PROCEDURE

Material

A titanium - 8-percent-aluminum - 1-percent-molybdenum - 1-percent-vanadium (Ti-8Al-1Mo-1V) alloy in the mill-annealed condition (1450^{o} F (790^{o} C) for 1 hour, air cooled) was used in this investigation. The chemical analysis and mechanical properties of the 1-inch- (2.5-cm-) diameter bar stock, as reported by the manufacturer, are as follows:

Chemical analysis, wt %:	
Al	7.8
Mo	1.0
V	1.0
C	0.023
Fe	0.05
N	0.011
O	0.07
H	0.007
Ti	Balance
Yield strength, ksi; MN/m^2	142; 978
Ultimate tensile strength, ksi; MN/m^2	148; 1020
Elongation, percent	20
Reduction of area, percent	40

Mechanical properties determined at Lewis on machined, tubular specimens of this material were as follows: elongation, 18 percent; reduction of area, 33 percent (based on outside diameter only); and ultimate tensile strength, 150 ksi (1034 MN/m^2). These properties compare favorably with those given by the manufacturer.

Threshold curves and creep data from the literature (ref. 11), as well as a limited amount of creep and stress-rupture data determined at Lewis, are presented in figure 1 for reference purposes.

Specimens

Tubular tensile specimens of the type illustrated in figure 2 were used in this investigation. The specimens were machined from as-received bar stock to a surface finish less than 10 microinches (0.25 μm) rms. They received no subsequent treatments other than cleaning with acetone and distilled water immediately prior to being coated with salt or subjected to hydrogenation.

Salt coating. - One series of specimens was coated prior to stress-corrosion testing with chemically pure sodium chloride. The average coating amounted to about 0.5 milligram per square inch (0.08 mg/cm^2). The salt was deposited on the bore of the tubular specimen. The technique and the dynamic air salting apparatus are fully described in references 11 and 12.

Thermal hydrogenation. - Another series of specimens was annealed at 1100° to 1200° F (590° to 650° C) in hydrogen gas. The pressure was about 17 psia (0.12 MN/m^2) and the annealing times were up to 2 hours. These annealing conditions resulted in the absorption of various hydrogen contents in the specimens.

Test Procedure

Creep exposure plus room-temperature tensile testing. - Subsequent to being salt coated, specimens were exposed at 800° F (427° C) in static air furnaces. They were exposed for about 100 hours at stress levels to 60 ksi (414 MN/m^2). After exposure, the creep specimens were tensile tested at room temperature at a crosshead speed of 5×10^{-3} inch per minute (1×10^{-2} cm/min) to determine residual ductility. Specimens were considered to be embrittled if the residual elongation was less than 15 percent and the reduction of area less than 25 percent, as compared to 18 and 33 percent, respectively, for the as-received material. These criteria are discussed in detail in reference 10.

Stress-rupture testing. - Salt-coated stress-rupture specimens were also exposed at 800° F (427° C) in static air furnaces. They were stressed at 80 ksi (551 MN/m^2) until failure.

Elevated-temperature tensile testing. - Salt-coated specimens were tensile tested at 600°, 700°, and 800° F (316°, 371°, and 427° C). The tensile crosshead speeds were 5×10^{-5}, 5×10^{-4}, and 5×10^{-3} inch per minute (1×10^{-4}, 1×10^{-3}, and 1×10^{-2} cm/min). Hydrogenated specimens were tested at 800° F (427° C) and 5×10^{-4} inch per minute (1×10^{-3} cm/min). All tensile tests were started approximately 1 hour after insertion of the specimen into the furnace.

The reduction-of-area data for all types of tests were determined from changes in outside diameter only. Elongation data were measured over a 1.00-inch (2.54-cm) gage length. A complete listing of all tests conducted is presented in tables I and II.

Chemical Analyses and Metallography

Hydrogen analyses. - Two independent laboratories used different techniques to analyze for hydrogen contents of selected specimens. Standard vacuum-fusion chemical analyses were made of many specimens. Small samples (0.05 g) were cut from regions immediately adjacent to the fracture surfaces of the broken halves of the specimens. Repeated analyses of the as-received alloy (70 ppm) indicated the precision at about ±15 ppm.

Ion-probe mass-spectrometric techniques were also used to determine local hydrogen concentrations in several specimens. The reported operating conditions were an accelerating potential of 10 kV, an energy window of 250 eV, a sputtering rate of 3.7 micrometers per minute, and a beam collimation of 22 micrometers.

Metallography. - The fracture surfaces of all salt-coated specimens were examined optically for evidence of stress-corrosion cracks. Minute cracks were easily identified because they were covered with blue corrosion products. Electron fractographic replicating techniques were used to ascertain the fracture modes of selected specimens. Scanning electron microscopy was also used to examine various aspects of the embrittlement of both hot-salt stress-corroded and hydrogenated specimens.

RESULTS AND DISCUSSION

Hot-Salt Stress-Corrosion Tests

Creep exposure plus room-temperature tensile tests. - There are several types of tests that can be used to demonstrate the deleterious effects of hot-salt stress-corrosion.

The most common type of test procedure is creep exposure. It involves a 100-hour exposure of a statically loaded, salt-coated titanium alloy specimen in the temperature range 500° to 900° F (260° to 480° C). Postexposure evaluation methods vary considerably among investigators. Threshold curves have been defined on the basis of corrosion products, cracks, and residual ductility. The author has previously demonstrated that residual ductility determined by a room-temperature tensile test at a low crosshead speed of 5×10^{-3} inch per minute (1×10^{-2} cm/min) is a very sensitive technique for determining the occurrence of stress-corrosion (refs. 10 and 11). The greater sensitivity of this technique is illustrated in figure 3. The plot of exposure stress against exposure temperature indicates the varying degrees of stress-corrosion damage that can be determined. The embrittlement threshold reveals that the initial effects of stress-corrosion are first noticed at very low stress levels. For example, after exposure at 800° F (427° C), embrittlement was determined at an exposure stress level of only 10 ksi (69 MN/m^2); see also table I. Not until the exposure stress exceeded 50 ksi (345 MN/m^2) were stress-corrosion cracks observed. These cracks were discolored due to either heat-tinting or corrosion products. Limited testing had suggested that exposure in excess of 100 hours would result in a shift of these thresholds to somewhat lower stress levels.

Stress-rupture tests. - As can be seen from figure 3 and table I, when the exposure stress was increased to 80 ksi (551 MN/m^2) at 800° F (427° C), specimens failed during exposure in a brittle manner. The failure times of the two specimens tested were 285 and 505 hours, as compared to the unsalted rupture life of over 1000 hours. It is assumed that stress-corrosion failures would occur within 100 hours if the exposure stress were increased to about 85 ksi (586 MN/m^2). For comparison, the normal 100-hour stress-rupture capability of the as-received alloy at 800° F (427° C) is about 100 ksi (689 MN/m^2); see figure 1.

Elevated-temperature tensile tests. - Another type of test that can be used to determine the effects of hot-salt stress-corrosion is an elevated-temperature tensile test. Salt-coated specimens were tested at 600°, 700°, and 800° F (316°, 371°, and 427° C). The tensile crosshead speeds were 5×10^{-5}, 5×10^{-4}, and 5×10^{-3} inch per minute (1×10^{-4}, 1×10^{-3}, and 1×10^{-2} cm/min). The results of these tensile tests are presented in figure 4 and table I. Both the elongation and reduction-of-area data for unsalted and salted specimens are plotted as a function of the tensile crosshead speed at the three test temperatures. In addition, the percentage of the cross-sectional area that was cracked and covered with corrosion products is indicated by the numbers adjacent to the data points in figure 4(b). It is evident from these data that severe embrittlement and cracking occurred during most of these tests. Damage was particularly severe at the lowest test speeds. For example, the specimen tested at 800° F (427° C) at 5×10^{-5} inch per minute (1×10^{-4} cm/min) exhibited only 25 percent of its unsalted reduction of area. About 37 percent of its fracture surface had cracked and was covered with corrosion products.

It is important to point out that the lowest crosshead speed, 5×10^{-5} inch per minute (1×10^{-4} cm/min), resulted in a total test time of about 80 hours. Obviously, this low-strain-rate test is not a conventional tensile test. Although the stress levels were low during the initial stages of the tensile test, in the final stages the specimens were exposed to stress levels similar to the stress-rupture conditions discussed previously. Consequently, it is not unexpected that a severe degree of embrittlement and cracking was encountered at these low tensile-test speeds. However, a substantial amount of cracking and embrittlement occurred even when the test speed was increased to 5×10^{-3} inch per minute (1×10^{-2} cm/min). These particular specimens were exposed at elevated temperatures for short periods of time. Temperature equilibrium was achieved within 1 hour and the total tensile-test time was about 1 hour. The tensile stresses were significantly high only during the last 40 minutes of the tensile test.

Test temperature was also an important variable. For example, the specimen tested at 700° F (371° C) and 5×10^{-3} inch per minute (1×10^{-2} cm/min) exhibited approximately 90 percent of its normal reduction of area. However, when the test temperature was increased to 800° F (427° C) at the same high crosshead speed, the specimen was embrittled to such a degree that it exhibited approximately 70 percent of its normal ductility. In addition about 5 percent of cross-sectional area of the specimen tested at 800° F (427° C) had cracked during the tensile test and was covered with corrosion products.

Metallography. - A photomacrograph of a hot-salt stress-corrosion failure is presented in figure 5. This specimen was exposed at 800° F (427° C) at 80 ksi (551 MN/m^2) until it failed after 285 hours. The appearance of the fracture surface of this specimen is typical of all stress-rupture and elevated-temperature tensile failures studied in this investigation. Of course, the creep specimens which are exposed at stresses below the crack threshold (fig. 3) do not exhibit the ring of cracked material near the specimen bore.

The details of the appearance of the fracture surface of the same specimen can be dramatically revealed by electron fractographic replicating techniques. Figure 6 illustrates that the fracture surface consists of three distinct zones. The zone nearest the salt-coated bore of the specimen fractured in a brittle manner (fig. 6(a)). This region of slow crack growth and secondary cracking is severely corroded and corresponds to the dark ring of material evident in figure 5. Farther away from the bore of the specimen, there is another zone that also fractured in a brittle manner (fig. 6(b)). However, this region of mixed intergranular and transgranular fracture is not covered with corrosion products. Ductile failure due to overload occurred in the region near the outer diameter of the tubular specimen. This region is characterized by the dimple pattern seen in figure 6(c), which is typical of the appearance of the fracture surfaces of unsalted, as-received specimens.

These three distinct zones were observed on the fracture surfaces of all salt-coated specimens that failed in either stress-rupture or elevated-temperature tensile tests. Specimens that were creep-exposed below the crack threshold and subsequently tensile tested to failure at room temperature exhibited only the zones shown in figures 6(b) and (c), as reported in a previous investigation (ref. 10).

The appearance of the intermediate zone of fractured material (fig. 6(b)) is particularly significant. This area of the specimen failed in a brittle manner, as indicated by the flat, cleavage-like regions. There is also some evidence of secondary cracking out of the plane of the fracture surface. However, the lack of evidence of any corrosion products indicates that this zone of material cracked before any corrosion occurred. This suggests that this region may have been embrittled by some species that diffused ahead of the main corrosion front. A similar observation that the crack tip was not corroded has been reported in reference 8.

A replica of an etched, longitudinal section of the specimen referred to in figure 6 is presented in figure 7. This electronmicrograph vividly illustrates the intergranular nature of the corrosion in the region near the salt-coated bore of the specimen and corresponds to the corroded brittle zone of figure 6(a). Both alpha-alpha and alpha-beta interfaces are preferentially attacked. The gross corrosion of the alloy nearest the salt-coated bore of the specimen is also evident.

The fracture surfaces of several stress-corroded specimens were also studied by scanning electron microscopy. This technique minimizes the introduction of artifacts on the fracture surface and has a much greater depth of field than replicating techniques. The results obtained for the salt-coated specimen tensile tested at 800° F (427° C) at the highest crosshead speed, 5×10^{-3} inch per minute (1×10^{-2} cm/min), are presented in figure 8. The cracked and corroded zone occurs immediately adjacent to the bore of the specimen (fig. 8(a)). This zone of intergranular corrosion is approximately 0.003 inch (0.008 cm) wide, or about 5 percent of the total cross-sectional area, as discussed previously. A brittle zone occurred next to the corrosion zone, although it was not continuous in this specimen. This brittle zone is evident in various portions of figures 8(b) and (c). Of course, the bulk of the fracture surface exhibited the honeycomb, or dimple, pattern which is typical of a ductile fracture (fig. 8(d).

Scanning microscopy also revealed some fine particles that were not observed with replicating techniques (fig. 8(b)). Although it was not possible to identify these particles, they may be involved in the embrittling mechanism. The significance of these particles will be discussed later in this report (see section Hydrogen Embrittlement Tests).

Hydrogen Analyses

Vacuum-fusion chemical analyses. - Most of the specimens tested in this investigation were analyzed for hydrogen content after they were exposed to the stress-corrosion test conditions. A thin ring of material was cut from the region immediately adjacent to the fracture surface of the stress-corroded specimens. The rings were approximately 0.1 inch (0.2 cm) thick and weighed about 0.05 gram. This size sample represents the minimum size required by the vendor for accurate analysis.

The hydrogen contents of some stress-corroded specimens were found to be significantly higher than that of the as-received titanium alloy (70±15 ppm). Specifically, several creep-exposed specimens contained up to 126 ppm, two stress-rupture specimens 111 to 255 ppm, and one elevated-temperature tensile-tested specimen 88 to 115 ppm (see table I).

It should be pointed out that these results represent the average hydrogen concentration of the entire sample selected for analysis. The difficulty of selecting a critical sample for analysis is evident from the hydrogen contents of the elevated-temperature tensile-tested specimens listed in table I. For instance, of the six most severely embrittled specimens submitted for analysis, only the one specimen tested at 800° F (427° C) at the lowest strain rate exhibited a hydrogen content above the base level of the as-received alloy. Previously reported data (ref. 10) also indicated that increases in hydrogen content could not be determined unless the analysis was made on small samples cut close to the fracture surface. It was speculated that hydrogen was concentrated near the fracture surface and that, if large samples were analyzed, these local concentrations of hydrogen were masked. They were averaged over the entire sample and thus approached the base-line value.

If, indeed, corrosion-produced hydrogen is segregated near the fracture surface, bulk chemical analyses would never be successful in determining precise concentrations. As a consequence, a new analytical method was used to determine hydrogen concentrations on a microscopic scale. The technique and the results obtained are described in the next section.

Ion-probe mass-spectrometric analyses. - Mass spectrometry was used to determine the composition of material sputtered off surfaces by a beam of argon ions collimated to 22 micrometers. As the ions hit the surface, they remove atoms and constantly expose new material. The beam gradually penetrates the sample at a rate controlled by the impingement of the argon ions. Thus, a concentration profile can be obtained for any element in the sample. We will be concerned only with hydrogen profiles in this investigation.

In order to determine the characteristics and accuracy of this technique, three samples were analyzed. One sample was taken from a longitudinal section of a tubular

specimen that had been thermally hydrogenated to about 4300 ppm. The other two samples were cut from the as-received bar stock (70 ppm). These samples were 1-inch (2.5-cm) disks about 0.2 inch (0.5 cm) thick. The as-received bar stock served as the basic standard from which all hydrogen concentrations were calculated.

The hydrogen profiles of these three samples are presented in figure 9. The hydrogen profile for the thermally hydrogenated sample agreed well with the bulk analysis determined by vacuum-fusion chemical techniques (4300 ppm). The measured concentrations of hydrogen ranged from 3600 to 6100 ppm over a depth of 86 micrometers.

The profiles for the two samples of as-received alloy exhibited good reproducibility even though the analyses were made several months apart. However, the relatively high hydrogen concentrations determined in the initial 100 micrometers below the surface are difficult to rationalize. Perhaps, local surface heating occurred during the cutting of samples from the bar stock and resulted in a nonuniform hydrogen distribution. It is also possible that these slight deviations and the overall gradient represent inherent instrumental and experimental error. Obviously, additional research is required to more fully define the accuracy of this new analytical technique.

Hydrogen profiles were determined on a specimen that had been creep exposed for 115 hours at 800° F (427° C) and 50 ksi (345 MN/m^2) and then tensile tested. Vacuum-fusion chemical tests had indicated the average bulk hydrogen content to be 90 to 126 ppm (see table I). Figure 10 illustrates the three transverse profiles (1, 2, and 3) and the two longitudinal profiles (4 and 5) that were made on a sample cut from the fracture surface of the creep-exposed specimen. High concentrations of hydrogen were measured near the fracture surface. Profile 3, which was measured closer to the fracture surface than profiles 1 or 2, revealed about 4500 ppm at a depth of 0.1 micrometer. The concentration profile gradually diminished to the base level of 70 ppm at a depth of about 4 micrometers. Neither profiles 1 nor 2 indicated any increase of hydrogen content over the base level. Both of the longitudinal profiles (4 and 5) indicated substantial hydrogen contents between depths of 1 to 10 micrometers below the fracture surface. Profile 5 even indicated several thousand ppm of hydrogen at depths 1 to 2 micrometers below the fracture surface in a region relatively close to the outer diameter of the specimen. Had profiles 4 and 5 been initiated at depths of less than 1 micrometer below the fracture surface, it is possible that even higher hydrogen contents would have been measured. There were no substantial deviations from base-level hydrogen content for any of these profiles between depths of 20 to 260 micrometers. Hence, these data are not represented on figure 10.

A more severely corroded stress-rupture specimen was also selected for analysis. This specimen had failed after 505 hours at 800° F (427° C) and 80 ksi (551 MN/m^2). Vacuum-fusion tests had indicated that the average bulk hydrogen content was 111 ppm (see table I). Both the sample and the regions of analysis were similar to those

discussed in connection with figure 10, and the hydrogen concentration profiles are shown in figure 11. Once again, for the three transverse profiles (1, 2, and 3) made along the bore of the salt-coated specimen, the hydrogen content increased substantially as the fracture surface was approached. Specifically, several thousand ppm were measured at various depths along profile 3, whereas only a few hundred ppm were measured along profiles 1 and 2. The two longitudinal profiles (4 and 5) indicated decreasing hydrogen concentrations as the analyses were made at increasing depths below the fracture surface, which was also true for the longitudinal profiles measured on the other specimen (fig. 10).

It is obvious from the results presented in figures 10 and 11 that additional research is necessary to determine completely and more accurately the distribution of hydrogen in these samples. For example, a contour map of hydrogen content could be determined if many additional profiles were analyzed. To clearly indicate the hydrogen distribution, these profiles should be close to each other and should extend from shallow depths of about 0.1 micrometer to several hundred micrometers below the salt-coated and fracture surfaces.

The limited data presented in this investigation confirm that corrosion-produced hydrogen is concentrated to extremely high levels near the intersection of the salt-coated bore and fracture surface. These tests conclusively demonstrate that hydrogen concentrations may be as much as two orders of magnitude greater than the average values determined by bulk chemical analyses. This suggests that corrosion-produced hydrogen is directly involved in the embrittlement and cracking observed during hot-salt stress-corrosion testing. The next section describes efforts to determine whether hydrogen alone, in the absence of a corrosive environment, could embrittle a titanium alloy in the temperature range where hot-salt stress-corrosion occurs.

Hydrogen Embrittlement Tests

Specimens were thermally hydrogenated to the high local concentration levels determined by the ion-probe mass-spectrometric tests reported in the previous section. These uniformly hydrogenated specimens were then tensile tested at 800° F (427° C) at a crosshead speed of 5×10^{-4} inch per minute (1×10^{-3} cm/min). These test conditions are identical to some of those used for the elevated-temperature tensile tests of salt-coated specimens described earlier in this report.

The tensile ductility of a series of specimens hydrogenated to various concentrations is presented in figure 12 and table II. As is evident from these data, hydrogen contents as great as about 2500 ppm had little effect on either reduction of area or elongation. Significant decreases in ductility were measured when the hydrogen content was

in the range 3000 to 4000 ppm. Still higher hydrogen concentrations, in the range 9000 to 12 000 ppm, resulted in complete embrittlement.

Specimens were examined both before and after tensile testing to ensure that hydrogenation did not result in cracking, which could have contributed to reduced strength and ductility. No cracks were evident after hydrogenation when the machined outer surfaces of the specimens were examined with fluorescent penetrant. In addition, post-tensile-test examination of the fracture surfaces near the inner and outer diameters of the specimen did not reveal any evidence of heat-tinted regions. If cracks had been induced by hydrogenation, heat tinting would have occurred during the elevated-temperature tensile test.

The fracture surface of a specimen hydrogenated to 12 000 ppm was examined by scanning electron microscopy. Two features were revealed that were similar to those observed on hot-salt stress-corroded specimens. The fractograph shown in figure 13 illustrates both the secondary cracking and the particles observed on the fracture surface of the hydrogenated specimen. The particles were assumed, but not confirmed, to be titanium hydride. Confirmation of their identity was not attempted because it is appreciated that the existence of a hydride phase at room temperature is not positive evidence that it precipitated at 800° F (427° C) where the brittle fracture occurred.

GENERAL REMARKS

Hydrogen Embrittlement Theories

Numerous investigations have been concerned with the embrittling effect of internal hydrogen on titanium alloys (refs. 13 to 17). However, none of these studies have reported any embrittling effect of hydrogen above temperatures of about 200° F (93° C). Embrittlement by internal hydrogen is manifested in two distinct types, designated impact embrittlement and low-strain-rate embrittlement.

Impact embrittlement. - This type of embrittlement is known to be due to the thermal precipitation of hydrides. It is most severe in α alloys. Embrittlement becomes more severe in the presence of a notch, at temperatures below ambient, at high strain rates, and with increasing hydrogen contents (refs. 13 and 14). This behavior is analogous to the classical problem of an increased ductile-brittle transition temperature.

Low-strain-rate embrittlement. - This form of embrittlement occurs at hydrogen contents less than those required for the thermal precipitation of hydrides. It is most common in $\alpha + \beta$ alloys, although it does occur in single-phase α and β alloys. Severity of embrittlement increases at higher hydrogen contents, at lower strain rates, and in a temperature range near ambient (refs. 13 to 17).

Low-strain-rate embrittlement is not completely understood, but it has been rationalized in terms of the diffusion-controlled segregation of hydrogen to preferred sites within the microstructure. These sites are most probably α-β interfaces. It is not clear whether this local segregation of hydrogen actually precipitates as a distinct hydride phase (refs. 13 and 15) or acts as dislocation pinning sites (refs. 16 and 17). At high strain rates, no embrittlement is observed because a critical concentration of hydrogen does not have sufficient time to develop. Similarly, a critical concentration is difficult to achieve at cryogenic temperatures where the diffusion rate of hydrogen is low. Likewise, a critical concentration is difficult to achieve at elevated temperatures because both the increased diffusion rate and the increased solubility tend to homogenize the hydrogen distribution. Of course, total hydrogen content influences both the strain rate and temperature ranges where embrittlement is maximized (ref. 13).

Stress-sorption embrittlement. - Corrosion-produced hydrogen has recently been suggested as the cause of cracking during hot-salt stress-corrosion of titanium alloys (refs. 3, 8, and 9). However, this theory of hydrogen embrittlement of titanium alloys differs from the internal-hydrogen theories discussed previously. This stress-sorption mechanism is analogous to one of the several classical theories that have been proposed for the hydrogen embrittlement of steels (ref. 18). The primary role of this external hydrogen is adsorption on crack surfaces, which results in weakened intermetallic bonds and enhanced crack propagation. However, these investigators do not reject the possibility that cracks may initiate at microscopic hydrides, although they have never observed any hydrides.

Hydrogen in Titanium Alloys

Although a limited amount of information about hydrogen solubility limits and diffusion rates is available for pure titanium, no information is available for the Ti-8Al-1Mo-1V alloy at elevated temperatures. Substantial differences in both solubility and diffusion rate probably exist due to the influence of the alloying elements and the β phase in the alloy. For example, the room-temperature solubility of hydrogen in pure titanium is about 10 ppm, but has been estimated at about 800 ppm for the Ti-8Al-1Mo-1V alloy at room temperature (ref. 19).

A recent study using autoradiographic techniques revealed that hydrogen diffuses to regions of high stress during creep exposure (ref. 20). A Ti-8Al-1Mo-1V alloy specimen with a varying cross section was charged with tritium to a uniform concentration of 275 ppm. Substantial amounts of tritium diffused to α-β interfaces at the regions of highest stress after a 200-hour exposure under load at 600° F (316° C). However, no distinct hydride phase was evident. The investigation of reference 20 has demonstrated

that applied stresses exert a dramatic effect on the diffusion and segregation of hydrogen in titanium alloys at elevated temperatures.

Significance of the Current Investigation

The results of this investigation have confirmed the postulate that corrosion-produced hydrogen is responsible for the elevated-temperature embrittlement of titanium alloys subjected to a hot-salt stress-corrosion exposure. It is probable that hydrogen can segregate to regions of stress concentration, such as corrosion pits and crack tips. This may be assumed based upon the investigation of reference 20. These regions of high hydrogen content result in embrittlement of titanium alloys.

However, the actual embrittling role of hydrogen has not been conclusively defined. The extremely high hydrogen concentrations determined slightly below the fracture surfaces of stress-corroded specimens are compatible with either the stress-sorption or internal-hydrogen embrittling mechanisms. However, an internal-hydrogen embrittling mechanism appears to be favored by the determination of significant concentrations of hydrogen at depths far below the salt-corroded and fracture surfaces. An internal-hydrogen embrittling mechanism is also favored by the temperature and strain-rate sensitivity exhibited during mechanical testing of creep-exposed specimens, as demonstrated by the author in reference 10.

Obviously, additional research is needed in order to conclusively define the actual embrittling role of hydrogen. The exact determination of the hydrogen solubility limit at 800° F (427° C) in the Ti-8Al-1Mo-1V alloy is an especially important experiment that should be performed. This information is vital in differentiating between the possible embrittling mechanisms. Mechanical testing in a gaseous hydrogen environment at 800° F (427° C) would also help to define the actual role of hydrogen in the process of hot-salt stress-corrosion of titanium alloys.

SUMMARY OF RESULTS

The purpose of this investigation was to determine if hydrogen could embrittle titanium alloys at high temperatures under conditions similar to hot-salt stress-corrosion exposures. Salt-coated specimens of the Ti-8Al-1Mo-1V alloy were tested in creep and stress-rupture, and by tensile tests in the temperature range 600° to 800° F (316° to 427° C). Severe embrittlement and/or cracking occurred for all types of tests. Both bulk and local hydrogen concentrations were determined in these stress-corroded specmens. Specimens hydrogenated to the measured local concentration levels were

mechanically tested at elevated temperatures. The following results were obtained:

1. Hydrogen can embrittle the Ti-8Al-1Mo-1V alloy during tensile testing at 800° F (427° C).

2. The concentration of thermally charged hydrogen required for full embrittlement is in the same range as the values measured near the fracture surfaces of specimens that had been subjected to hot-salt stress-corrosion exposures.

3. Local segregation of hydrogen up to several thousand ppm was measured near the fracture surface of stress-corroded specimens. The ion-probe mass-spectrometer used for these measurements appears to be a valuable tool for studying stress-corrosion problems.

4. Electron fractographic and scanning microscopic examinations of the fracture surfaces of hot-salt stress-corroded specimens supported the concept of hydrogen embrittlement. There was a noncorroded brittle zone of material between a corroded brittle zone and a ductile zone. This suggests that an embrittling species, such as hydrogen, diffused ahead of the main corrosion front.

5. This investigation has demonstrated that tensile tests conducted in the temperature range 600° to 800° F (316° to 427° C) can be used to supplement creep exposure and stress-rupture tests to study the influence of hot-salt stress-corrosion on titanium alloys. The obvious advantage is that information can be gained within a few hours instead of a hundred or more hours.

Lewis Research Center,
National Aeronautics and Space Administration,
Cleveland, Ohio, October 14, 1970,
129-03.

REFERENCES

1. Anon.: Stress-Corrosion Cracking of Titanium. Spec. Tech. Publ. No. 397, ASTM, 1966.

2. Gray, Hugh R.: Hot-Salt Stress-Corrosion of Titanium Alloys. Aerospace Structural Materials. NASA SP-227, 1970, pp. 251-268.

3. Rideout, S. P.; Louthan, M. R., Jr.; and Selby, C. L.: Basic Mechanisms of Stress-Corrosion Cracking of Titanium. Stress-Corrosion Cracking of Titanium. Spec. Tech. Publ. No. 397, ASTM, 1966, pp. 137-151.

4. Lingwall, R. G.; and Ripling, E. J.: Elevated Temperature Stress Corrosion of High Strength Sheet Materials in the Presence of Stress Concentrators. Material Research Lab., Inc. (NASA CR-88979), Aug. 1967.

5. Boyd, W. K.; and Fink, F. W.: The Phenomenon of Hot-Salt Stress-Corrosion Cracking of Titanium Alloys. NASA CR-117, 1964.

6. Petersen, V. C.; and Bomberger, H. B.: The Mechanism of Salt Attack on Titanium Alloys. Stress-Corrosion Cracking of Titanium. Spec. Tech. Publ. No. 397, ASTM, 1966, pp. 80-94.

7. Hatch, A. J.; Rosenberg, H. W.; and Erbin, E. F.: Effects of Environment on Cracking in Titanium Alloys. Stress-Corrosion Cracking of Titanium. Spec. Tech. Publ. No. 397, ASTM, 1966, pp. 122-136.

8. Rideout, S. P.; Ondrejcin, R. S.; Louthan, M. R.; and Rawl, D. E.: The Role of Moisture and Hydrogen in Hot-Salt Cracking of Titanium Alloys. Conference on Fundamental Aspects of Stress Corrosion Cracking. Nat. Assoc. Corrosion Eng., 1969, pp. 650-661.

9. Rideout, S. P.: The Initiation of Hot-Salt Stress Corrosion Cracking of Titanium Alloys. Applications Related Phenomena in Titanium Alloys. Spec. Tech. Publ. No. 432, ASTM, 1968, pp. 205-217.

10. Gray, H. R.: Hot Salt Stress Corrosion of a Titanium Alloy: Generation of Hydrogen and Its Embrittling Effect. Corrosion, vol. 25, no. 8, Aug. 1969, pp. 337-341.

11. Gray, Hugh R.; and Johnston, James R.: Hot-Salt Stress-Corrosion of a Titanium Alloy Under a Simulated Turbine-Engine Compressor Environment. NASA TN D-5510, 1969.

12. Gray, Hugh R.: Hot-Salt Stress-Corrosion of Titanium Alloys: Generation of Hydrogen and Its Embrittling Effect. NASA TN D-5000, 1969.

13. Williams, D. N.: The Hydrogen Embrittlement of Titanium Alloys. J. Inst. Metals, vol. 91, 1962-1963, pp. 147-152.

14. Cotterill, P.: The Hydrogen Embrittlement of Metals. Progress in Materials Science, vol. 9, no. 4. Pergamon Press, 1961, pp. 241-259.

15. Robinson, H. A.; Frost, P. D.; and Parris, W. M.: Effect of Hydrogen on Some Mechanical Properties of a Titanium Alloy Heat-Treated to High Strength. Trans. AIME, vol. 212, no. 4, Aug. 1958, pp. 464-469.

16. Daniels, R. D.; Quigg, R. J.; and Troiano, A. R.: Delayed Failure and Hydrogen Embrittlement in Titanium. ASM Trans., vol. 51, 1959, pp. 843-861.

17. Burte, Harris M.: Strain Aging Hydrogen Embrittlement in Alpha-Beta Titanium Alloys. Trans. Soc. Rheology, vol. 1, 1957, pp. 119-151.

18. Petch, N. J.; and Stables, P.: Delayed Fracture of Metals Under Static Load, Nature, vol. 169, May 17, 1952, pp. 842-843.

19. Boyd, J. D.: Precipitation of Hydrides in Titanium Alloys. ASM Trans. Quart., vol. 62, Dec. 1969, pp. 977-988.

20. Mackay, T. L.: Stress Corrosion Cracking of Titanium Alloys at Ambient Temperature in Aqueous Solutions. NASA CR-1464, 1969.

TABLE I. - SUMMARY OF HOT-SALT STRESS-CORROSION TEST DATA

(a) Hot-salt creep exposure tests

Specimen	Exposure conditions					Room-temperature tensile tests at 5×10^{-3} in./min (1×10^{-2} cm/min)							Hydrogen concentration, ppm
	Temperature		Time, hr	Stress		Ultimate stress		Fracture stress		Reduction of area, percent	Elongation, percent	Area cracked, percent	
	°F	°C		ksi	MN/m^2	ksi	MN/m^2	ksi	MN/m^2				
239	800	427	96	10	69	150	1034	144	992	27	17	--	---
30	↓	↓	↓	10	69	152	1048	150	1034	19	14	--	---
231				20	138	149	1027	139	958	27	18	--	---
36				20	138	148	1020	146	1006	19	14	--	---
234				30	207	153	1055	153	1055	11	7	--	---
18				50	345	152	1048	152	1048	10	8	--	86, 100
12			112	50	345	151	1041	150	1034	7	6	--	53, 60, 102
11			115	50	345	159	1096	159	1096	12	10	--	90, 126
111			96	50	345	153	1055	153	1055	16	8	<1	--- ---
97			93	60	414	145	999	145	999	7	3	1	---

(b) Hot-salt stress rupture tests

39	800	427	285	80	551	---	---	---	---	5	6	30	189, 255
106	↓	↓	505	↓	↓	---	---	---	---	14	10	33	111
[a]115			1055			---	---	---	---	51	35	--	70
[a]412			1981			---	---	---	---	51	38	--	70

(c) Hot-salt tensile tests

Specimen	Temperature		Crosshead speed		Ultimate stress		Fracture stress		Reduction of area, percent	Elongation, percent	Area cracked, percent	Hydrogen concentration, ppm
	°F	°C	in./min	cm/min	ksi	MN/m^2	ksi	MN/m^2				
[a]315	600	316	5×10^{-4}	1×10^{-3}	120	827	109	751	34	20	--	70
[a]291	↓	↓	5×10^{-4}	1×10^{-3}	118	813	105	723	39	20	--	70
[a]374			5×10^{-5}	1×10^{-4}	117	806	108	744	36	20	--	70
246			5×10^{-4}	1×10^{-3}	117	806	108	744	33	18	0	---
237			5×10^{-5}	1×10^{-4}	88	606	85	586	24	13	<1	54
[a]297	700	371	5×10^{-3}	1×10^{-2}	116	799	101	696	41	19	--	70
[a]221	↓	↓	5×10^{-4}	1×10^{-3}	112	772	98	676	40	21	--	70
[a]377			5×10^{-5}	1×10^{-4}	115	792	97	668	43	24	--	70
236			5×10^{-3}	1×10^{-2}	111	765	102	703	37	19	0	---
233			5×10^{-4}	1×10^{-3}	107	737	101	696	28	18	3	53, 53
306			5×10^{-5}	1×10^{-4}	112	772	106	730	19	15	18	63, 69
[a]283	800	427	5×10^{-3}	1×10^{-2}	114	785	106	730	43	24	--	70
[a]294	↓	↓	5×10^{-4}	1×10^{-3}	109	751	83	572	48	26	--	70
[a]228			5×10^{-5}	1×10^{-4}	117	806	67	462	54	33	--	70
235			5×10^{-3}	1×10^{-2}	103	710	94	647	31	17	5	52, 62
255			5×10^{-4}	1×10^{-3}	96	661	91	627	22	15	18	57, 58
230			5×10^{-5}	1×10^{-4}	68	468	59	407	13	10	37	88, 115

[a]Unsalted.

TABLE II. - SUMMARY OF TENSILE TEST DATA OF

HYDROGENATED SPECIMENS

[Temperature, 800° F (427° C); crosshead speed, 5×10^{-4} in./min (1×10^{-3} cm/min).]

Specimen	Hydrogen content,[a] ppm	Ultimate stress		Fracture stress		Reduction of area, percent	Elongation, percent
		ksi	MN/m^2	ksi	MN/m^2		
[b]294	70	109	751	83	572	48	26
[c]140	70	101	696	75	517	53	32
351	1 250	97	669	75	517	47	29
362	2 300	96	662	63	434	53	32
343	2 350	98	676	67	462	50	25
352	2 500	86	593	55	379	52	25
405	3 500	91	628	64	441	47	15
368	3 800	98	676	53	365	44	13
378	3 950	99	682	52	358	52	19
394	9 700	43	296	43	296	0	0
404	11 400	68	469	68	469	↓	0
360	12 200	54	372	54	372		0
342	12 300	98	676	98	676		2

[a]Average of two or more determinations.

[b]As received.

[c]Annealed in argon at 1200° F (650° C) for 1 hr.

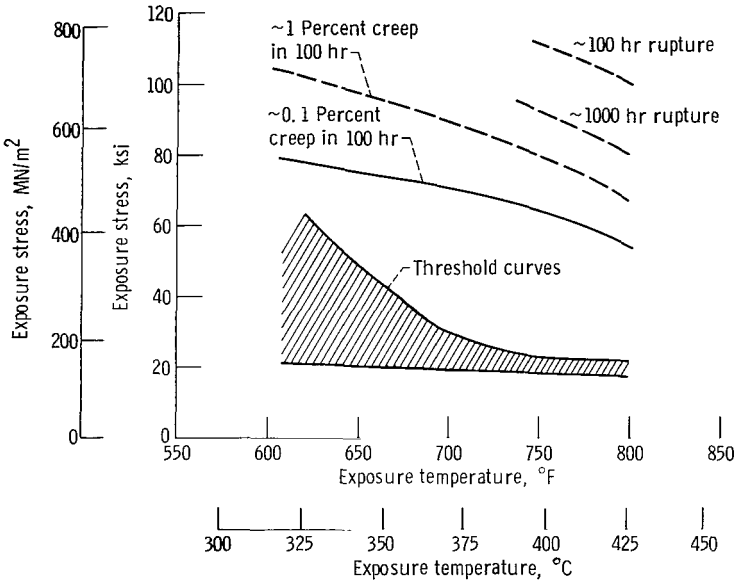

Figure 1. - Baseline creep, stress-rupture, and hot-salt stress-corrosion threshold data for Ti-8Al-1Mo-1V alloy (ref. 11).

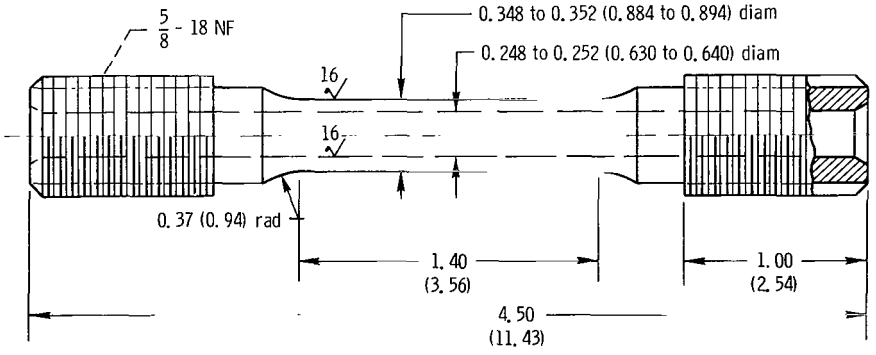

Figure 2. - Tubular, titanium alloy, tensile specimen used in hot-salt stress-corrosion investigation. (All dimensions are in inches (cm).)

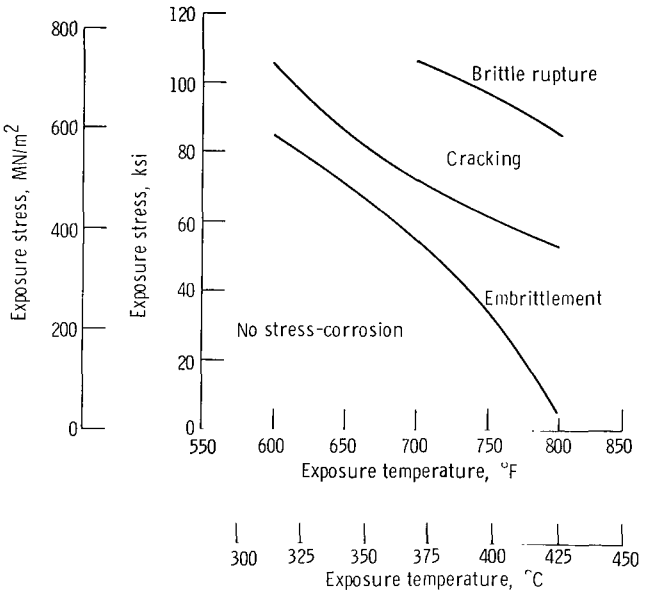

Figure 3. - Types of 100-hour hot-salt stress-corrosion damage for Ti-8Al-1Mo-1V alloy specimens salt-coated at 400° F (204° C).

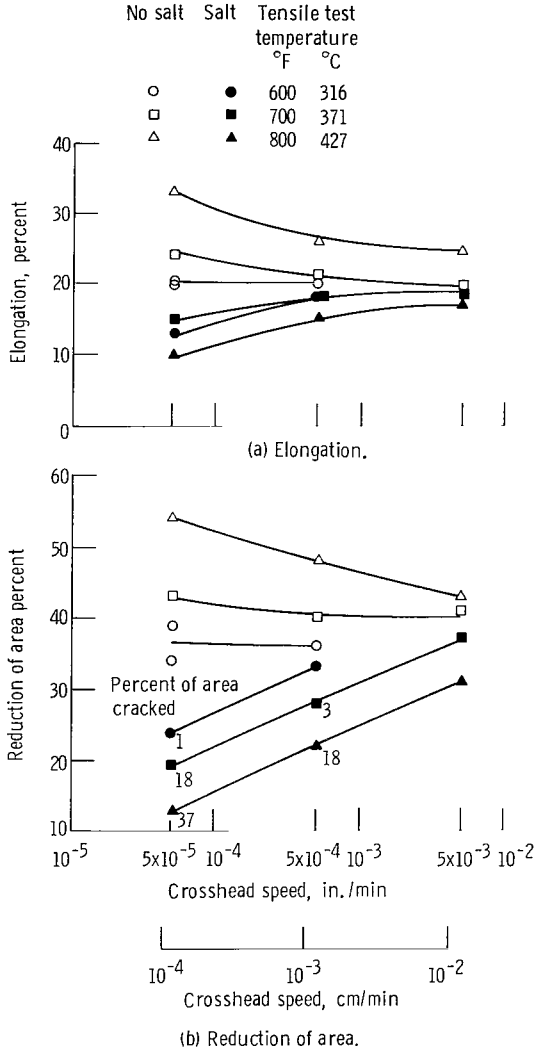

Figure 4. - Elevated temperature tensile ductility of Ti-8Al-1Mo-1V alloy specimens. Salt-coated at 400° F (204° C); no subsequent exposure.

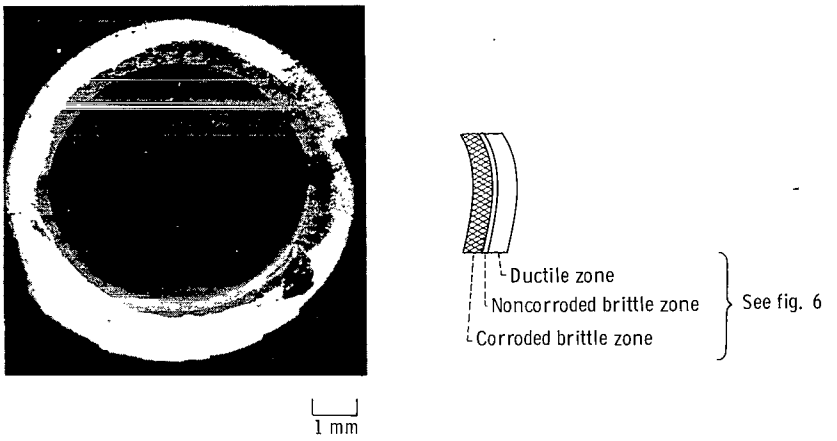

Figure 5. - Fracture surface of hot-salt stress rupture specimen. (800° F (427° C), 80 ksi (551 MN/m^2), 285 hours.

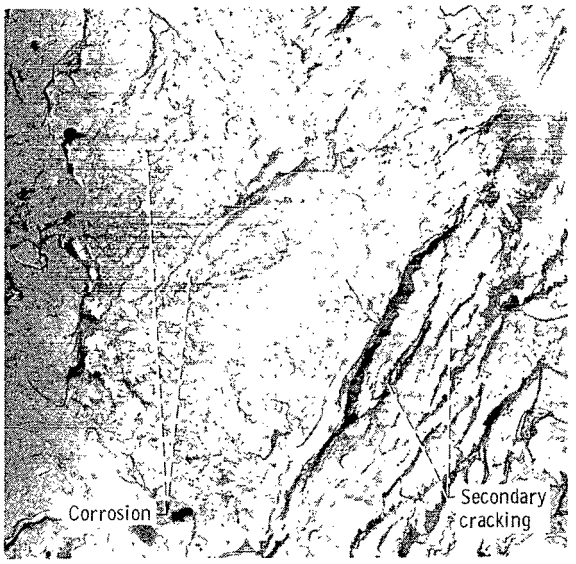

(a) Slow-crack-growth zone. (Note severe corrosion and secondary cracking out of fracture plane.)

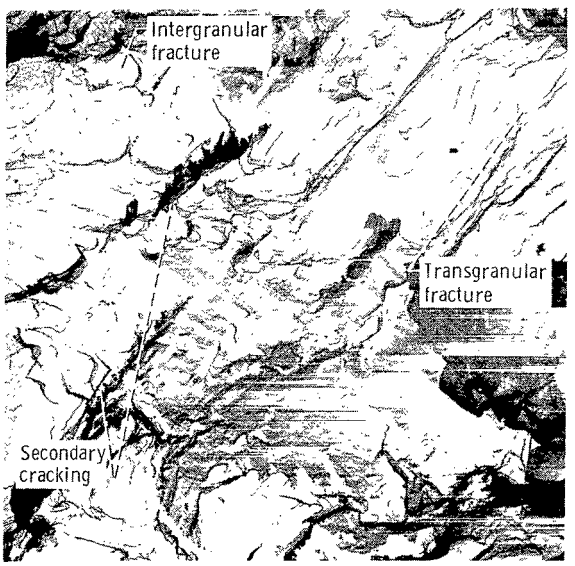

(b) Intermediate brittle zone of mixed intergranular and transgranular fracture. (Note absence of corrosion.)

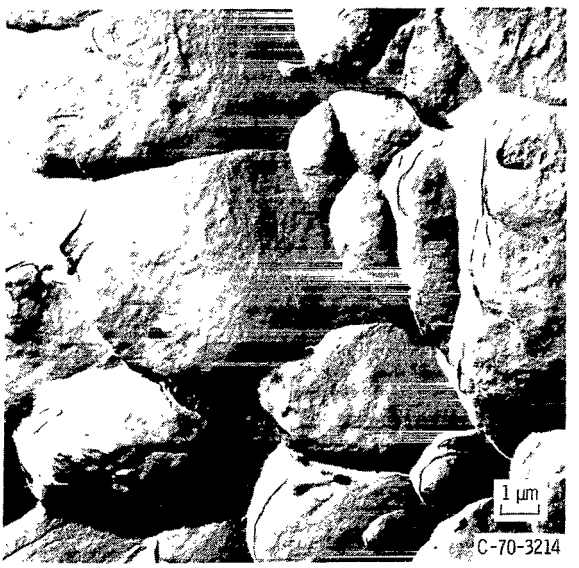

(c) Ductile overload zone of fracture surface.

Figure 6. - Electron fractographs of hot-salt stress-rupture specimen. Temperature, 800° F (427° C); stress, 80 ksi (551 MN/m^2) for 285 hours.

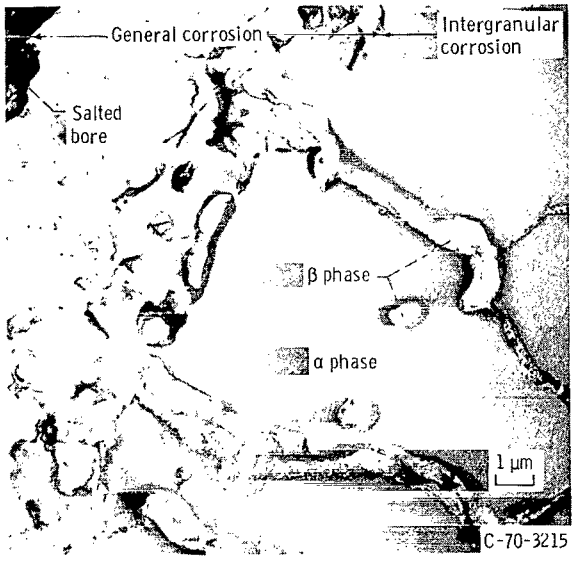

Figure 7. - Electron replica of etched, longitudinal section near bore of hot-salt stress-rupture specimen. (Note severe general corrosion and intergranular corrosion.) Temperature, 800° F (427° C); stress, 80 ksi (551 MN/m^2) for 285 hours.

(a) Intergranular corrosion zone, transition zone, and ductile matrix.

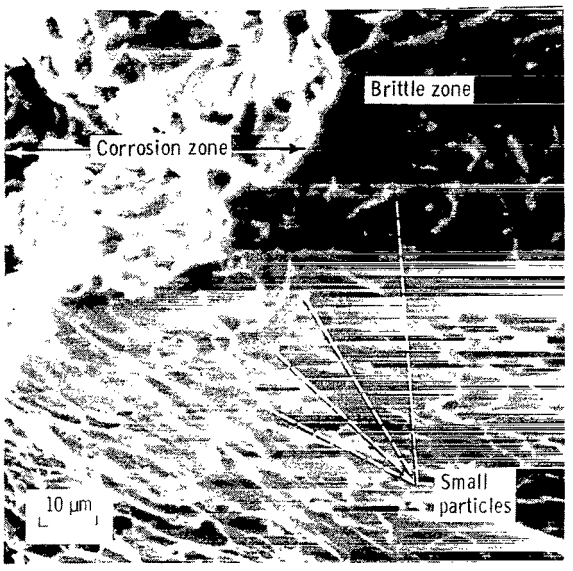

(b) Brittle transition zone showing small particles.

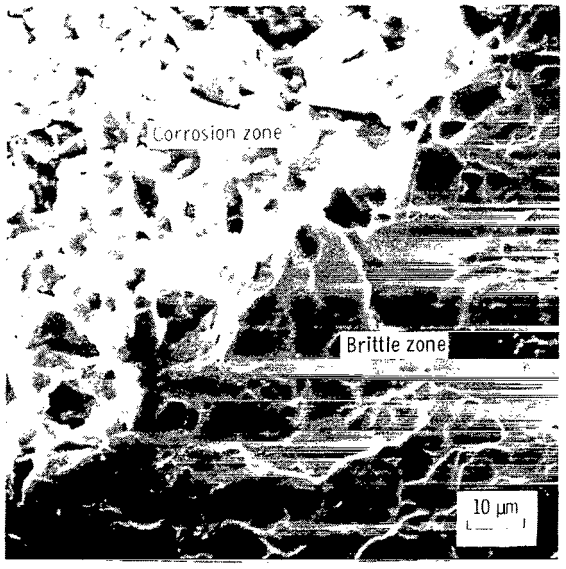

(c) Brittle transition zone.

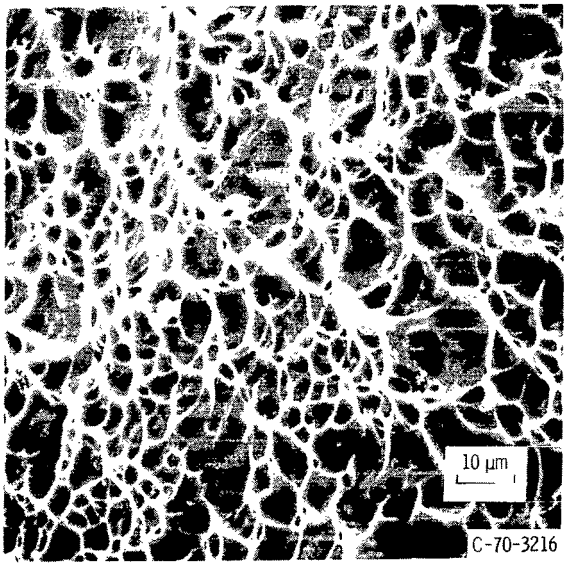

(d) Dimple pattern typical of ductile matrix.

Figure 8. - Scanning electron micrographs of fracture surface of hot-salt tensile-tested specimen. Temperature, 800° F (427° C); crosshead speed, 5×10^{-3} inch per minute (1×10^{-2} cm/min).

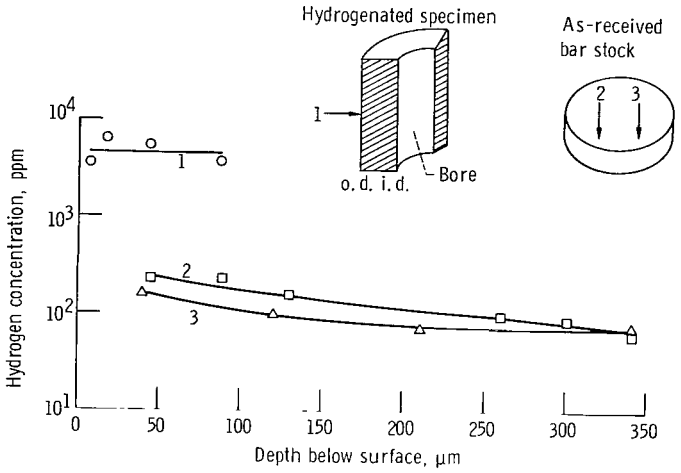

Figure 9. - Hydrogen concentration profiles for as-received standard (70 ppm) and thermally hydrogenated specimen (4300 ppm).

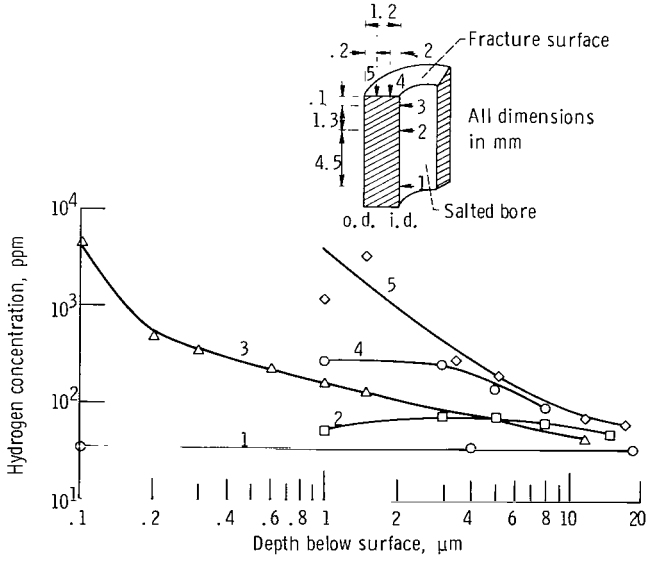

Figure 10. - Hydrogen concentration profiles for creep-exposed specimen. Temperature, 800° F (427° C); stress, 50 ksi (345 MN/m^2) for 115 hours; hydrogen content, 90 to 126 ppm.

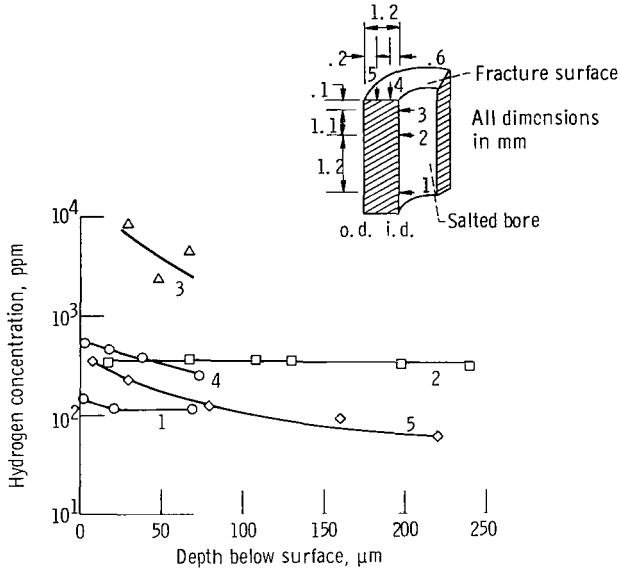

Figure 11. - Hydrogen concentration profiles for stress-rupture specimen. Temperature, 800° F (427° C); stress, 80 ksi (551 MN/m^2) for 505 hours; hydrogen content, 111 ppm.

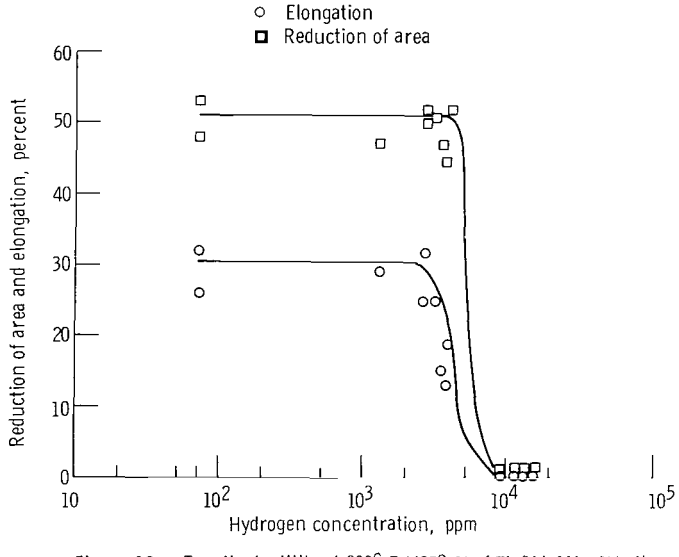

Figure 12. - Tensile ductility at 800° F (427° C) of Ti-8Al-1Mo-1V alloy specimens hydrogenated at 1200° F (650° C). Tensile crosshead speed, $5x10^{-4}$ inch per minute ($1x10^{-3}$ cm/min).

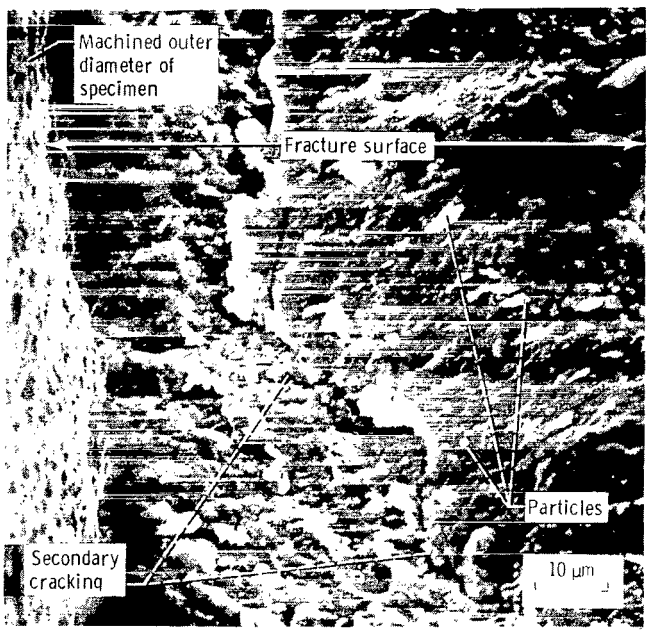

C-70-3217

Figure 13. - Scanning electron micrograph of fracture surface of specimen thermally hydrogenated at 1200° F (650° C) to 12 000 ppm. (Note particles on fracture surface and secondary cracking out of fracture plane).

NATIONAL AERONAUTICS AND SPACE ADMINISTRATION
WASHINGTON, D. C. 20546
OFFICIAL BUSINESS

FIRST CLASS MAIL

POSTAGE AND FEES PAID
NATIONAL AERONAUTICS AND
SPACE ADMINISTRATION

"The aeronautical and space activities of the United States shall be conducted so as to contribute . . . to the expansion of human knowledge of phenomena in the atmosphere and space. The Administration shall provide for the widest practicable and appropriate dissemination of information concerning its activities and the results thereof."

—NATIONAL AERONAUTICS AND SPACE ACT OF 1958

NASA SCIENTIFIC AND TECHNICAL PUBLICATIONS

TECHNICAL REPORTS: Scientific and technical information considered important, complete, and a lasting contribution to existing knowledge.

TECHNICAL NOTES: Information less broad in scope but nevertheless of importance as a contribution to existing knowledge.

TECHNICAL MEMORANDUMS: Information receiving limited distribution because of preliminary data, security classification, or other reasons.

CONTRACTOR REPORTS: Scientific and technical information generated under a NASA contract or grant and considered an important contribution to existing knowledge.

TECHNICAL TRANSLATIONS: Information published in a foreign language considered to merit NASA distribution in English.

SPECIAL PUBLICATIONS: Information derived from or of value to NASA activities. Publications include conference proceedings, monographs, data compilations, handbooks, sourcebooks, and special bibliographies.

TECHNOLOGY UTILIZATION PUBLICATIONS: Information on technology used by NASA that may be of particular interest in commercial and other non-aerospace applications. Publications include Tech Briefs, Technology Utilization Reports and Technology Surveys.

Details on the availability of these publications may be obtained from:

SCIENTIFIC AND TECHNICAL INFORMATION OFFICE

NATIONAL AERONAUTICS AND SPACE ADMINISTRATION

Washington, D.C. 20546